Chapter 4 Thermal Sensitive Quantum Confinement of MoS_2 Nanostructures

4.1 Introduction

Now a day's numerous techniques are employed to find the semiconducting nature of materials. The examination of the surface with electrons or ions to observe characteristic change of specimen and providing electrical contacts to the device can be used for identifying semiconducting nature, which may act as destructive technique. However, the optical techniques are non-destructive, contactless and sensitive for the same. Photoluminescence (PL) is one of the optically sensitive technique to analyse the semiconducting nature of materials [163-166]. In case of TMDs, d-electrons' interactions can give rise to photoluminescence (PL) [167]. Quantum confinement behaviour of TMDs nanostructured can be understood by examining their electronic bandgap, which is a key to determine the transport and optical properties of these materials. A tunable bandgap would be highly desirable as it allows great flexibility to make an optoelectronic device for wide range applications [163]. In general, TMDs nanostructures show indirect-to-direct bandgap transition when transformed from bulk to monolayer/few-layer due to interlayer coupling [6]. Among the family of TMDs, MoS_2 is known to be stable and environment-friendly layered material, which can be used in different electronic, optoelectronic and sensor devices. The PL of MoS_2 can also be modulated by external stimuli such as pressure, temperature, strain etc for promising use in light sensitive applications [47, 126, 154].

In literature, few studies were performed for temperature dependent PL of MoS_2. Li *et al.* synthesized triangular monolayer MoS_2 over three different substrate and

found that PL intensity reduces with increasing temperature due to thermal quenching [168]. Hu *et al.* observed thermally produced strain in monolayer MoS_2 due to mismatch of thermal expansion coefficients of monolayer MoS_2 and the substrate [169]. Lu *et al.* studied the temperature dependent PL study of single layer MoS_2 and found that the PL intensity increases with decreasing temperature [144]. In the present work, we are examining the temperature response of quantum confinement to understand the optical properties of triangular bilayer MoS_2 and vertically oriented few-layer MoS_2 (VFL-MoS_2) using temperature dependent PL spectroscopy. The schematic representation of this study is shown in **Figure 4.1.** We demonstrate the enhanced photoluminescence at low temperatures of prepared MoS_2 nanostructures, suggesting their suitability for optoelectronics devices. These two films show good tunability of bandgap with temperature. The tunable bandgap in MoS_2 justify their use in future optical and nanoelectronics devices.

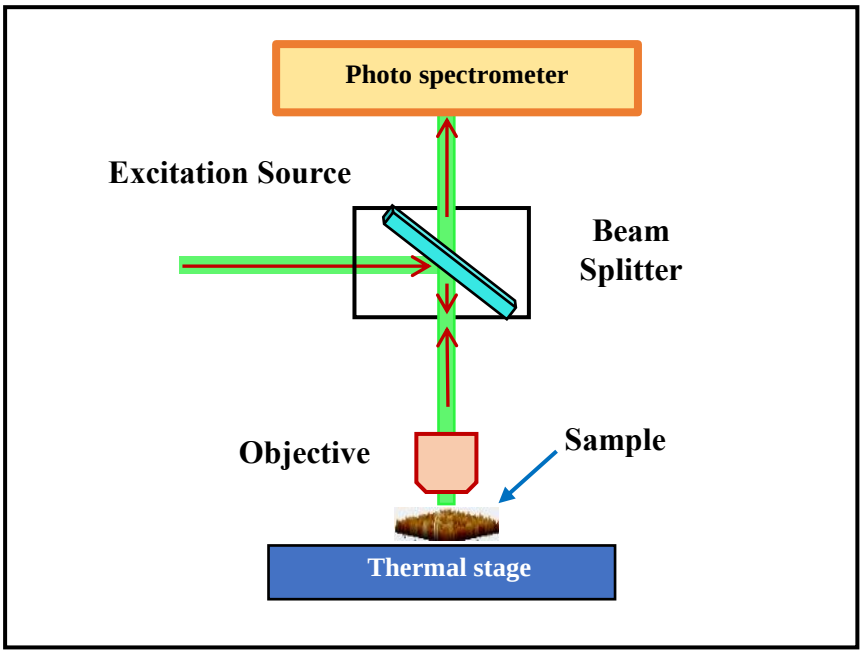

Figure 4.1 *Schematic diagram of the temperature dependent PL measurement process.*

4.1.1 Origin of Photoluminescence and Variation of Bandgap in 2D Materials

Strong light-matter interactions are predictable in 2D nanomaterials, such as direct to indirect transition in semiconducting MoS_2. The strongly coupled electron-hole pairs (excitons) are generated due to the coulomb interaction upon optical excitation of 2D material. Lifetime of these excitons depends upon the crystal lattice, impurity concentration and type, defects etc. Eventually the excitons will recombine either radiatively or non-radiatively. The radiative emission is known as photoluminescence (PL). Different possible transitions including excitation and emission are shown schematically in **Figure 4.2**. The first emission shown in **Figure 4.2** is band-to-band recombination. Those materials possess small effective masses owing to the large electron orbital radii shows this kind of transitions, which are rarely seen. Another radiative mechanism is free-exciton recombination. This radiative transition observed from defect free sample. The third radiative mechanism corresponds to transition of excitons bounded to shallow donors, while fourth radiative mechanism belongs to free-electron-to-acceptor transitions [170]. The energy of the radiation is determined by the binding energies of the donors and acceptors. The last transition is involved with an acceptor donor pair is shown in the right most part of **Figure 4.2**.

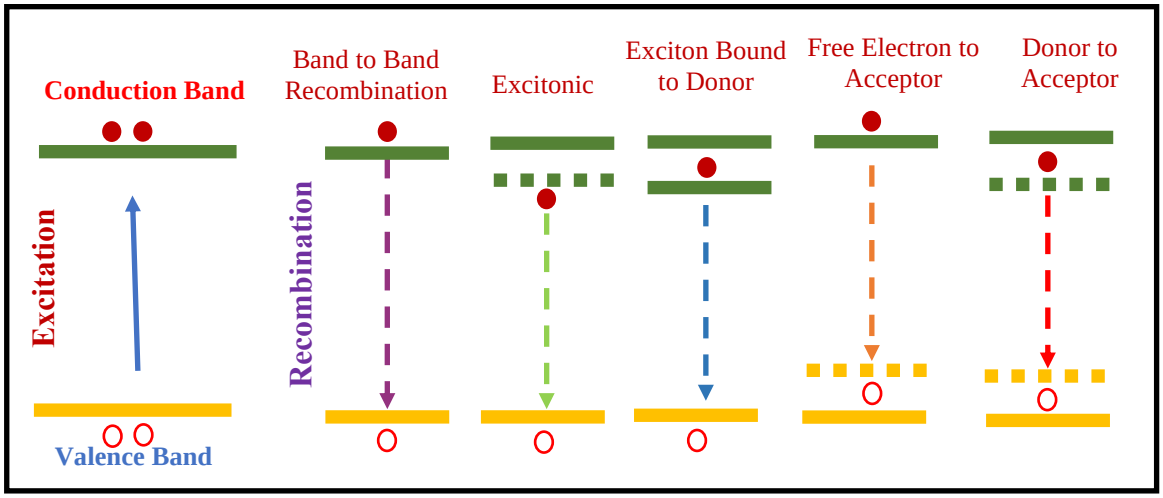

Figure 4.2 *Common transitions in photoluminescence process [170].*

The stacking of TMD layers provides different electronic properties. It has been observed that the electronic bandgap and the band structure of TMDs depends on the coordination environments of the transition metals, interactions of *d*-electrons and the stacking sequence [167]. The nature of layered TMDs can be metallic, semi-metallic or semiconducting with direct or indirect bandgaps depending on their phase and layer numbers. The monolayer semiconducting TMDs shows perfect direct transition. The electronic structures of TMDs depends on interlayer coupling, quantum confinement, and symmetry, when transformed from bulk to few-layer or monolayer TMDs. Experimentally it has been found that the intensity of A and B excitonic peaks decreases with the increasing layer numbers due to the transition from direct to indirect bandgap [6, 14, 168]. However, the energies of these peaks (peak positions) show weak dependence on the layer number. On the other hand, it has been found that the indirect bandgap of TMDs shows a redshift of 200-300 meV, when it transforms from bilayer to bulk. The energy of the indirect transition can be fitted with the quantum well like expression as follows [171] -

$$E_I^{(N)} = E_0 + \hbar^2\pi^2/2\mu L^2 \tag{4.1}$$

where $E_I^{(N)}$ represent the indirect bandgap of 2D materials with N layers and E_0 represent the bandgap of bulk materials. The $\hbar$ and μ are the Planck's constant and reduced electron–hole effective mass, respectively. The thickness of the 2D materials is defined as L= Na, where N is the layer number and a is the thickness of the monolayer 2D materials. In layered 2D materials, the bandgap is usually reduced as the number of layers increases [171, 172].

4.2 Results and Discussion

4.2.1 Origin of Photoluminescence in MoS_2 Nanostructures

Among different 2D TMDs materials, few-layer/monolayer MoS_2 has several unique characteristics compared to bulk MoS_2 [167]. The excitonic states become highly luminescent in case of monolayer and few-layer MoS_2 compared to that for bulk phase of MoS_2. In MoS_2 nanostructures, PL peak is observed due to the direct electronic transitions resulting in higher radiative recombination rate as compared to the non-radiative recombination rate. The PL quantum efficiency in MoS_2 arises from the direct excitonic state and it can be expresses as follows [167] -

$$\eta_{Lum} = \frac{k_{rad}}{k_{rad}+k_{defect}+k_{relax}} \quad (4.2)$$

where k_{rad}, k_{defect} and k_{relax} represent the rates of radiative recombination, defect trapping, and electron relaxation between the conduction and valence bands, respectively. In case of bulk MoS_2 the intra-band relaxation rate is very high, hence the PL from the direct excitonic transitions is not observed in bulk. The PL intensity enhanced in few-layer/monolayer due to the slower electronic relaxation k_{relax}. In thinner MoS_2, the intra-band relaxation rate from the excitonic states decreases due to the increase in the indirect bandgap resulting in stronger PL. The PL spectrum of MoS_2 at room temperature mainly shows two peaks in the visible range corresponding to the direct A and B excitons [173, 174]. The spin-orbit coupling leads to the valence band splitting at K point of Brillouin zone resulting in two distinct emission features corresponding to the ground state exciton (strong A-peak) and higher spin-orbit split state (weak B-peak), as shown schematically in **Figure 4.3.** The energy difference between A and B peak provides the spin-orbit energy.

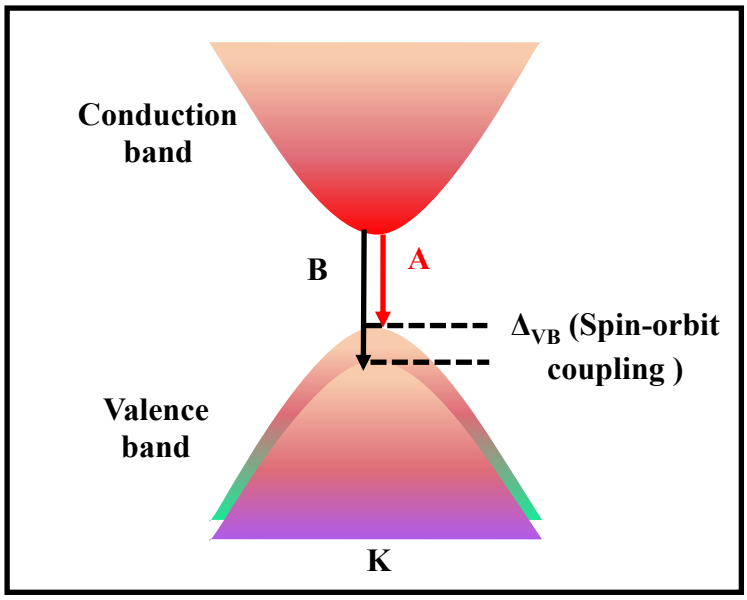

Figure 4.3 *A schematic representation of A and B excitons in 2D materials.*

In the present chapter, we have studied the photoluminescence properties of two different morphologies of MoS_2 nanostructures, which are horizontally grown triangular bilayer MoS_2 and vertically oriented few-layer (VFL) MoS_2. The optical image of horizontally grown triangular bi-layer MoS_2 over SiO_2/Si substrate is shown in **Figure 4.4 (a)** and corresponding room temperature gaussian fitted PL spectrum is given in **Figure 4.4 (b)**. It shows two direct excitons A and B, at 690 nm and 638 nm, respectively. The intensity of A exciton is higher as compared to the B exciton. The SEM of prepared VFL-MoS_2 over Si substrate is shown in **Figure 4.4 (c)**, suggesting vertical morphology of MoS_2 nanostructures and the corresponding room temperature PL spectrum of VFL-MoS_2 nanosheets is given in **Figure 4.4 (d)**, which clearly indicates the presence of A (~678 nm) and B (-638 nm) excitons (peak positions via Gauss fitting). In following section, we have discussed the temperature dependent quantum confinement behaviour of these MoS_2 nanostructures by studying their temperature response of PL.

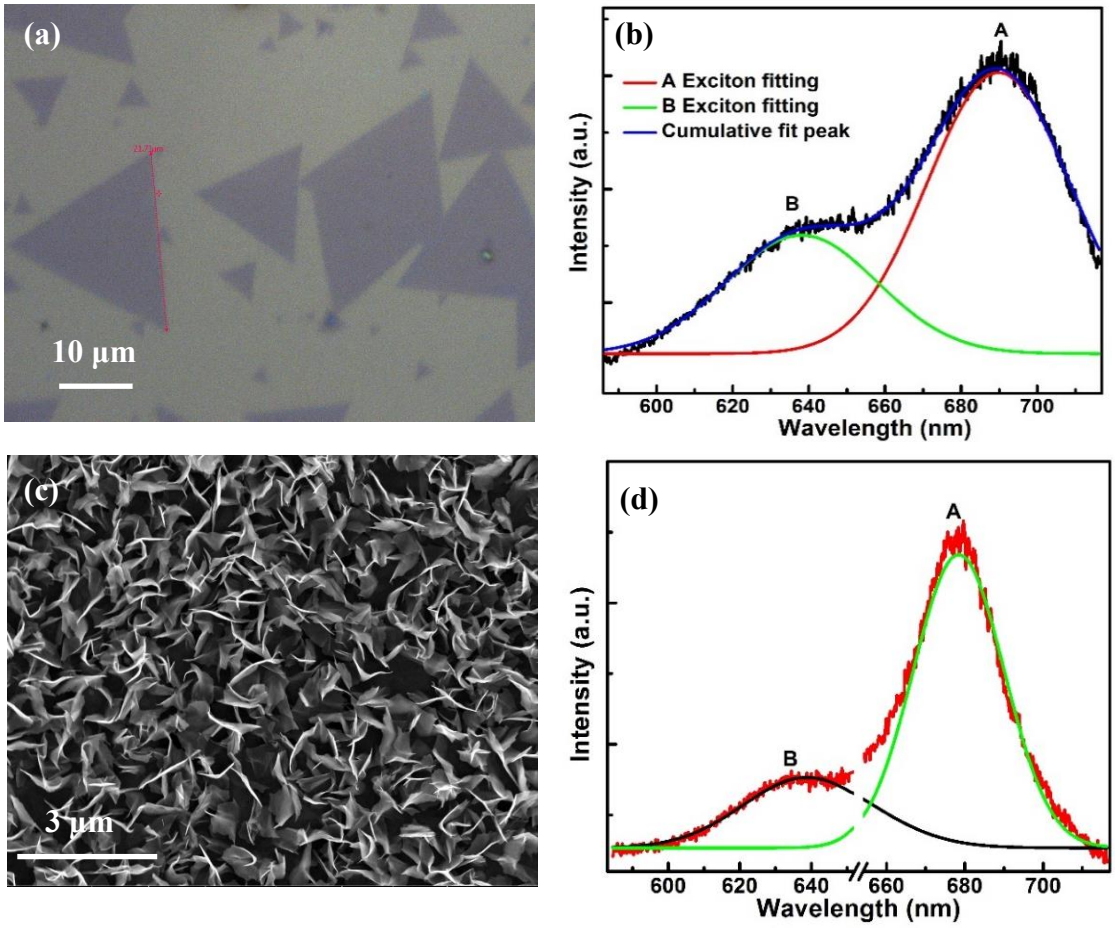

Figure 4.4 *(a) Optical image of triangular bi-layer MoS_2 over SiO_2/Si substrate. (b) Room temperature PL spectra (Gaussian fitted) of triangular bi-layer MoS_2 over SiO_2/Si substrate (c) SEM image of vertically oriented few-layer MoS_2 nanosheets (d) Room temperature PL spectra (Gaussian fitted) of VFL- MoS_2 over Si substrate.*

4.2.2 Temperature Dependent PL Study of Horizontally Grown Triangular Shaped Bi-Layer MoS_2

In order to examine the tunable nature of bandgap of MoS_2 nanostructure, we have performed temperature dependent PL study from low temperature (83 K) to room temperature (300 K) for triangular bi-layer MoS_2 nanostructure over SiO_2/Si substrate. The optical image of studied triangular bi-layer MoS_2 over SiO_2/Si substrate is shown in **Figure 4.5 (a)**. The experimental measured PL peaks represents the nature of excitons and the lower bounds on the fundamental bandgap values in semiconducting nanostructures. The Gaussian fitted PL spectra for triangular bi-layer MoS_2 at different

temperatures in the temperature range 300 K to 83 K are shown in **Figure 4.5 (b)**. The PL spectrum at room temperature shows two peaks around 690 nm and 638 nm, corresponding to the direct A and B excitons, respectively, occurring due to the spin-orbit coupling effect [174, 175]. We found that as the temperature increases from 83 K to 300 K, both the excitons intensity reduces and excitons are red shifted due to the expansion of bond length, lattice constant, increase in electron-phonon and phonon-phonon scattering [176]. We clearly observe that the integrated PL intensity (area under the curve for A exciton) also decreases with increasing temperature (**Figure 4.5c**) according to following Arrhenius equation [176, 177] -

$$I(T) = \frac{1}{1+A_1 \exp\left(-\frac{E_{A1}}{k_b T}\right)} \tag{4.3}$$

where *I(T)* is the temperature-dependent PL intensity and A_1 is the constant related to the densities of non-radiative recombination centers of the materials. The E_{A1}, is the activation energy corresponding to nonradiative channels of the materials and k_B is the Boltzmann constant. The obtained values of A_1 and E_{A1} are 2.23 and 31.38 meV, respectively. Further we analyzed the temperature dependent PL intensities of triangular bi-layer MoS_2 of A excitons, which can be explained by the following relation [178] -

$$I(T) = \frac{I_0 \times k_{rad}(T)}{k_{rad}(T)+k_{nonrad}(T)} \tag{4.4}$$

where I(T) is the PL intensity of the system at temperature T and I_0 is the maximum PL intensity at low temperature. The $k_{rad}(T)$ is the temperature dependent radiative recombination rate and $k_{nonrad}(T)$ is the temperature dependent non-radiative recombination rate. At high temperature the electron–phonon interactions increases and due to that the thermally activated non-radiative recombination increases, resulting in decrease in PL intensity with enhanced temperature [48, 179].

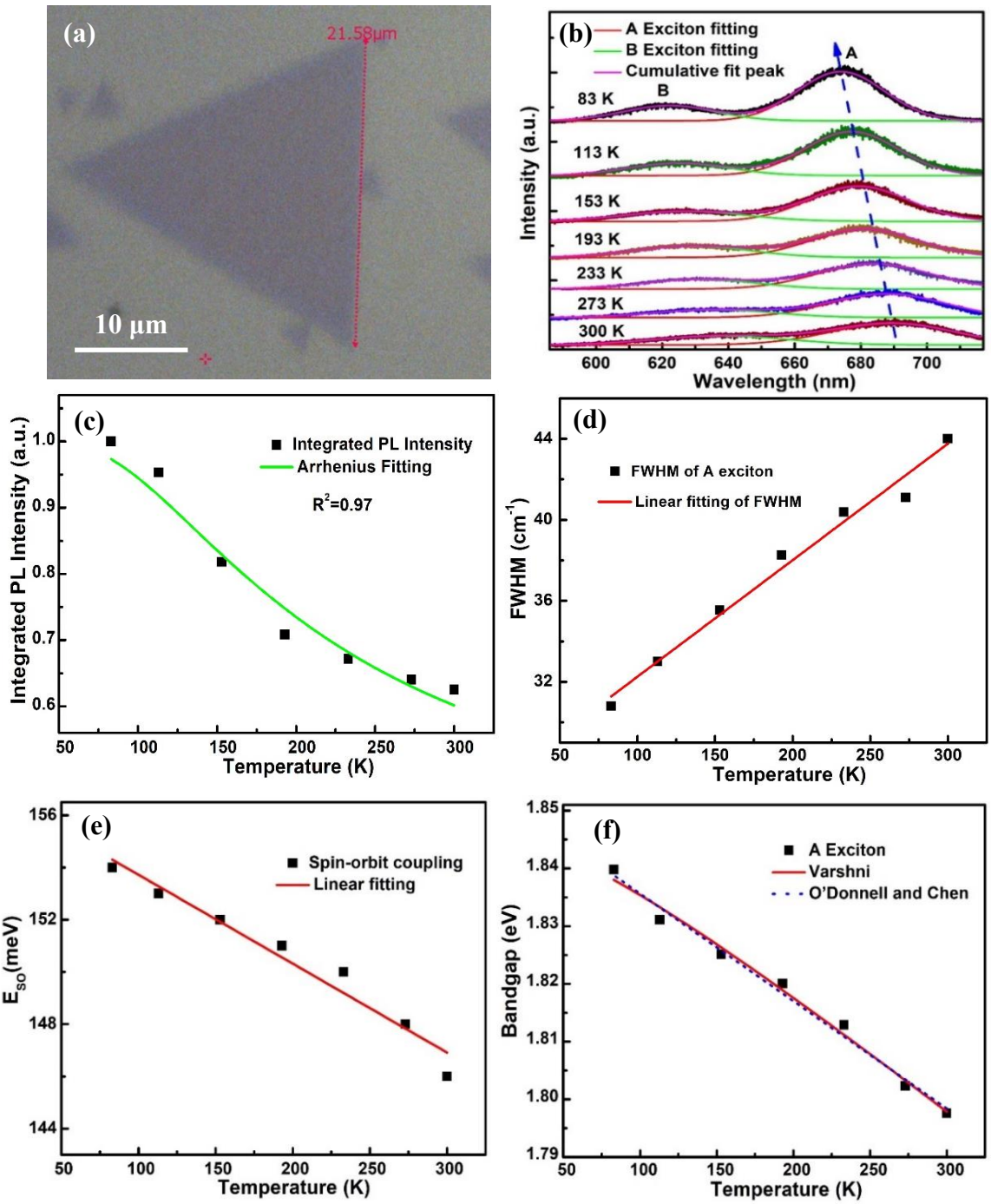

Figure 4.5 *(a) Optical image of triangular bi-layer MoS_2 over SiO_2/Si substrate. (b) Gaussian fitted PL spectra of triangular bi-layer MoS_2 on SiO_2/Si substrate at different temperatures. Variation of (c) Total PL intensity (d) FWHM for A exciton with temperature. (e) Variation of spin-orbit splitting between A and B exciton with temperature. (f) Fitting of variation in bandgap with temperature.*

In MoS_2 nanostructure the bandgap reduction is observed with the enhanced temperature which attributed to the enhanced electron–phonon interactions along with the lattice dilation at higher temperature. The full width at half maxima (FWHM) for A

exciton increases linearly with increasing temperature as shown in **Figure 4.5 (d)** due to defect related inhomogeneous broadening and enhanced phonon-exciton interaction. At room temperature (300 K), a separation of 146 meV is observed between A and B exciton, which increases to 151 meV and 154 meV, at 193 K and 83 K, respectively. The separation between A and B exciton roughly gives an idea about the spin-orbit splitting and our observation indicates that spin-orbit splitting energy decreases with increasing temperature as shown in **Figure 4.5 (e)**. At higher temperatures, lattice vibrations are enhanced which result in increased electron-phonon scattering and non-radiative process leading to increased FWHM and decreased PL intensity [179].

Further we observe the variation of minimum direct bandgap for triangular bi-layer MoS_2 film on SiO_2/Si substrate with temperature, as shown in **Figure 4.5 (f)**. The bandgap of bi-layer MoS_2 decreases with the increasing temperature as observed in conventional semiconducting materials. We use two different models, Varshni equation and O'Donnell and Chen equation, to fit the variation of bandgap with temperature [180, 181]. The Varshni equation can be expressed as follows [180] -

$$E_g(T) = E_g(0) - \frac{\alpha T^2}{(T+\beta)} \tag{4.5}$$

where $E_g(T)$ and $E_g(0)$ represent the energy of A exciton at temperature T and 0 K, respectively. The α is the bandgap energy temperature coefficient and β is the Debye temperature of the materials. The fitting parameters provide value of $E_g(0) = 1.84\ eV$, $\alpha = 2.19 \times 10^{-4}\ eV/K$ and β = 105.5 K for the A exciton. To know about the electron-phonon coupling constant (S) and the average energy of the phonon $\langle \hbar\omega \rangle$, we fit the variation of bandgap by one more hyperbolic cotangent formula based on electron-phonon coupling, called as O'Donnell and Chen equation. This equation can be expressed as follows [181] -

$$E_g(T) = E_g(0) - S\langle\hbar\omega\rangle\left[Coth\left(\frac{\langle\hbar\omega\rangle}{2k_BT}\right) - 1\right] \quad (4.6)$$

This equation additionally provides the information about the density of phonons at certain temperature (hyperbolic function), average phonon energy ($\langle\hbar\omega\rangle$) and electron-phonon coupling (constant S).[50] We have found the value of $E_g(0)$ = 1.85 eV, S =1.08 and $\langle\hbar\omega\rangle$ = 19.0 meV. The energy bandgap of triangular bilayer MoS_2 decreases (central wavelengths of the A exciton is red-shifted) with increasing temperature due to enhanced electron-phonon scattering and lattice expansion [48].

4.2.3 Temperature Dependent PL Study of Vertically Grown Few-Layer MoS_2

The high-resolution SEM image of the VFL-MoS_2 is shown in **Figure 4.6 (a)**. The SEM image of VFL-MoS_2 shows that MoS_2 nanosheets are grown in the vertical direction i.e. perpendicular to the silicon substrate. We performed the temperature dependent PL study of prepared VFL-MoS_2 nanostructure to observed the tunable nature of bandgap. The spin-orbit coupling leads to the valence band splitting resulting in two distinct emission features corresponding to the ground state exciton (strong A-peak) and higher spin-orbit split state (weak B-peak) [173]. **Figure 4.6 (b)** shows the PL spectra of VFL-MoS_2 from room temperature to lower temperature (293 K to 113 K). The strong A exciton shows significant blueshift in exciton energy with enhanced intensities at decreasing temperatures. Higher PL intensities are observed at lower temperatures due to increased radiative recombination of the exciton decay processes. The observed blue shift can be attributed to the temperature dependent squeezing of the lattice and electron-lattice interaction at low temperature [144, 169]. The integrated PL intensity (area under the curve for A exciton) follows Arrhenius **equation 4.3** and decreases with increasing temperature, as shown in **Figure 4.6 (c)**, due to the increased electron-phonon interaction leading to more non-radiative recombination. We have fitted the PL intensity of A exciton

and found the value of A_1~ 2.56 and E_{A1}~ 50.55 meV. We also found that the FWHM for A exciton of VFL-MoS_2 increases linearly with increasing temperature as shown in **Figure 4.6 (d)**. At higher temperatures, lattice vibrations are enhanced leading to increased electron-phonon scattering, phonon-exciton interaction and defect related inhomogeneous broadening, which result in increased FWHM. Further, we have observed the variation of spin-orbit splitting energy with respect to the temperature as shown in **Figure 4.6 (e)**. The energy difference of the two excitons at 293 K is found to be around 130 meV in VFL-MoS_2 sample, which increases to 138 meV at low temperature of 113 K. The spin-orbit splitting energy of VFL-MoS_2 is found increasing at lower temperatures. We have further observed the variation of bandgap energy of A exciton with respect to the temperature. We have found that as the temperature of the system increases the bandgap energy value decreases due to the lattice dilation effect [164]. The variation of minimum bandgap for VFL-MoS_2 film on Si substrate with temperature is shown in **Figure 4.6 (f)**. Again, we have used two models- Varshni equation and O'Donnell and Chen equation, to fit the variation of bandgap with temperature [180, 181]. The red line in **Figure 4.6 (f)** shows the Varshni fitting and it gives the fitted values of $E_g(0) = 1.90\ eV,\ \alpha = 3.32 \times 10^{-4}\ eV/K$ and β = 110 K for the A exciton. The O'Donnell and Chen equation provides the direct information about dependency of bandgap with temperature, average phonon energy ($\langle \hbar\omega \rangle$) and electron-phonon coupling for semiconducting behaviour [181, 182]. The fitted dotted line in **Figure 4.6 (f)** shows the O'Donnell and Chen fitting, which provides the $E_g(0)$ = 1.90 eV, S=1.68 and $\langle \hbar\omega \rangle$ = 4.1 meV. Hence, temperature dependent PL study suggests the tunable nature of semiconducting VFL- MoS_2 nanosheets, in which bandgap depends upon temperature.

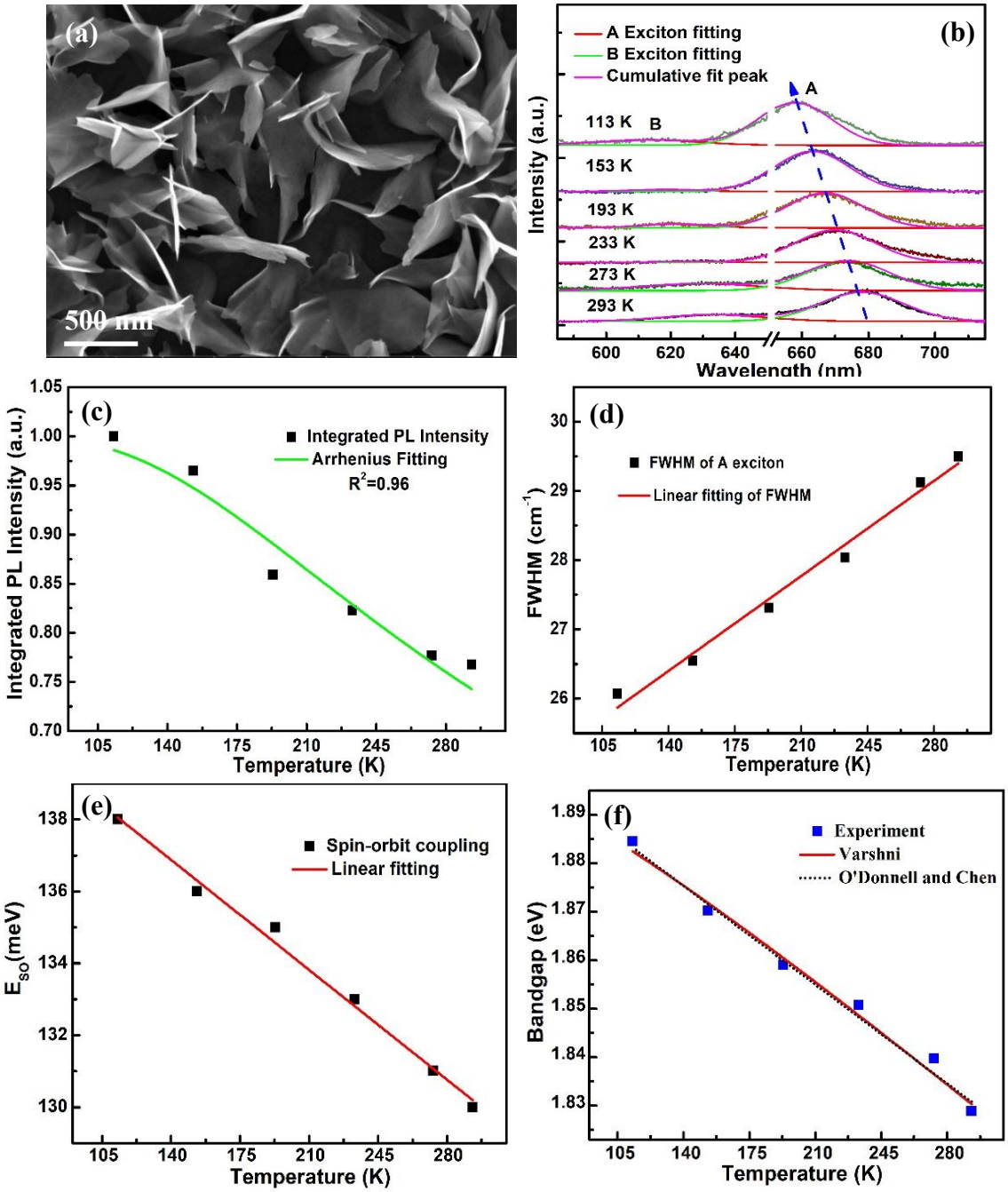

Figure 4.6 *(a) SEM image of VFL-MoS_2 (b) Gaussian fitted PL spectra of VFL-MoS_2 on Si substrate at different temperatures. Variation of (c) Total PL intensity (d) FWHM for A exciton with temperature for VFL-MoS_2. Variation of (e) Spin-orbit splitting between A and B exciton with temperature of VFL-MoS_2. (f) Fitting of variation in bandgap with temperature of VFL-MoS_2.*

4.3 Conclusions

We have successfully demonstrated the photoluminescence behaviour of two different morphologies of semiconducting MoS_2 nanostructure. We analyzed the temperature dependent PL behaviour of horizontally grown triangular bi-layer MoS_2 and VFL-MoS_2 nanostructures. We demonstrate the enhanced photoluminescence at low temperatures for both MoS_2 nanostructures due to the more radiative recombination and reduced electron-phonon interaction. At higher temperatures, lattice vibrations are enhanced, which results in increased electron-phonon scattering and non-radiation process leading to increased FWHM and decreased PL intensity. The presence of direct excitons may facilitate the use of MoS_2 nanostructures for optoelectronic and photonic applications such as photodetection and SERS applications. This study concludes that synthesized triangular bi-layer MoS_2 and VFL-MoS_2 shows excellent semiconducting nature with tunable bandgap in response to physical stimuli such as temperature, which can be suitable as tunable bandgap material for application in photodetector, solar cell, display technology, transistor etc.